Helmholtz-Zentrum Dresden-Rossendorf (HZDR)

Characterizing the Ionization Potential Depression in Dense Carbon Plasmas with High-Precision Spectrally Resolved X-ray Scattering

Kraus, D.; Bachmann, B.; Barbrel, B.; Falcone, R. W.; Fletcher, L. B.; Frydrych, S.; Gamboa, E. J.; Gauthier, M.; Gericke, D. O.; Glenzer, S. H.; Göde, S.; Granados, E.; Hartley, N. J.; Helfrich, J.; Lee, H. J.; Ravasio, A.; Nagler, B.; Schumaker, W.; Vorberger, J.; Döppner, T.;

Perma-Link to Publication Repository of HZDR:

https://www.hzdr.de/publications/Publ-27704

Characterizing the Ionization Potential Depression in Dense Carbon Plasmas with High-Precision Spectrally Resolved X-ray Scattering

D. Kraus[1,2], B. Bachmann[3], B. Barbrel[4], R. W. Falcone[4], L. B. Fletcher[5], S. Frydrych[6], E. J. Gamboa[5], M. Gauthier[5], D. O. Gericke[7], S. H. Glenzer[5], S. Göde[5], E. Granados[5], N. J. Hartley[1], J. Helfrich[6], H. J. Lee[5], A. Ravasio[8], B. Nagler[5], W. Schumaker[5], J. Vorberger[1], T. Döppner[3]

[1]Helmholtz-Zentrum Dresden-Rossendorf, Bautzner Landstr. 400, 01328 Dresden, Germany
[2]Institute of Solid State and Materials Physics, Technische Universität Dresden, 01069 Dresden, Germany
[3]Lawrence Livermore National Laboratory, Livermore, CA 94550, USA
[4]Department of Physics, University of California, Berkeley CA 94720, USA
[5]SLAC National Accelerator Laboratory, Menlo Park CA 94309, USA
[6]Institut für Kernphysik, Technische Universität Darmstadt, Schlossgartenstraße 9, 64289 Darmstadt, Germany
[7]CFSA, Department of Physics, University of Warwick, Coventry CV4 7AL, United Kingdom
[8]LULI, UMR7605, CNRS-CEA, Université Paris VI-Ecole Polytechnique, 91128 Palaiseau Cedex, France

E-mail: `d.kraus@hzdr.de`

July 2018

Abstract. We discuss the possibility of obtaining highly precise measurements of the ionization potential depression in dense plasmas with spectrally resolved X-ray scattering, while simultaneously determining the electron temperature and the free electron density. A proof-of-principle experiment at the Linac Coherent Light Source, probing isochorically heated carbon samples, demonstrates the capabilities of this method and motivates future experiments at X-ray free electron laser facilities.

1. Introduction

The complex properties of dense plasmas play a crucial role in our understanding of celestial bodies like giant planets, brown dwarfs and stars as well as scientific and technological applications like intense laser-matter interaction (both optical and X-ray), fusion energy studies and radiation damage research [1].

Ionization is a key quantity of every plasma. In dense matter, the bound states, and accordingly the ionization balance, are modified by the interaction with the surrounding medium. In particular, the influence of neighboring ions and screening due to continuum electrons results in reduced binding strength, which can be modeled by introducing effective (lower) ionization energies (ionization potential depression, IPD). Although a precise description of the complex interaction of a dense plasma including bound states remains difficult, the Stewart & Pyatt model [2], which interpolates between well-known low-density, high-temperature (Debye-Hueckel) and high-density, low-temperature (ion sphere) limits, is thought to catch most of the essential physics and is widely applied. However, several experiments have recently challenged this method, indicating a significantly larger depression of the ionization energy [3, 4, 5], whereas other results are in line with this description [6]. This controversy motivated several more advanced model approaches [7, 8, 9], but so far, no final convergence has been reached [10].

What is still lacking, however, are experiments which can precisely measure electron temperature, free electron density (ionization) and IPD at the same time. In this article, we discuss very promising capabilities of high-precision spectrally resolved X-ray scattering, as now enabled by X-ray Free Electron Lasers, in order to address present controversies on this topic. Dense plasmas can be created by ultrafast isochoric heating with these highly brilliant X-ray sources [11]. Moreover, the X-rays can be applied to simultaneously characterize a set of plasma properties, particularly the IPD as well as ionization and electron temperature, with high-precision *in situ* spectrally resolved X-ray scattering. After introducing the basic concepts of this measurement technique focussing on the IPD measurement of dense carbon plasmas, we discuss a corresponding proof-of-principle experiment on isochorically heated graphite that was recently performed at the Linac Coherent Light Source (LCLS) of SLAC National Accelerator Larboratory and provides a first step forward towards future high-precision experiments.

2. Basic Concepts

Carbon has the highest melting temperature of all elements and is of high interest for isochoric heating experiments. Cold carbon is dominated by electronic band structure and only the K-shell electrons can be treated in an atomic approximation. When entering the warm dense matter regime at a few thousand kelvins, significant bonding remains [12], while some of the L-shell electrons may be treated atomically before entering a regime of significant ionization at higher temperatures. Reaching the dense plasma regime with temperatures of several eV, plasma physics can be applied to describe the system via ionic bound states, free electrons and IPD. In addition, carbon is probably the most practical low-Z material for experiments on dense plasma properties. In contrast to hydrogen, helium, nitrogen, oxygen, etc., it exists in a solid state at ambient conditions, which simplifies the experimental creation of solid-density plasmas. Moreover, its two ambient polymorphs, graphite (ρ=2.2 g/cm^3) and diamond (ρ=3.5 g/cm^3) allow for accessing conditions of different density by simply switching between these two forms of carbon as initial material. Furthermore, carbon is not as hazardous and difficult to handle as, e.g., beryllium or lithium. By using organic compounds as sample material, carbon can easily be studied in mixtures with light elements that are of high relevance for astrophysics [13] and fusion applications [14].

Many of the characteristic properties of dense plasmas are accessible by spectrally resolved X-ray scattering. In general, the scattered radiation power spectrum per solid angle is given by [15]

$$\frac{dP}{d\Omega\omega} = I_0 r_0^2 (1 - \cos^2\phi \sin^2\theta) N S(k,\omega), \qquad (1)$$

where I_0 is the initial probe intensity, r_0 the classical electron radius, ϕ the FEL polarization angle, θ the scattering angle, and N the number of atoms in the probe volume. $S(k,\omega)$ denotes the electron structure factor in dependence of scattering wave number k and frequency shift ω, and contains the microscopic properties of the sample. In a plasma, X-rays either scatter from single electrons (non-collective scattering) or from collective fluctuations of many electrons (collective scattering), depending on the scattering geometry applied in the experiment [16]. The scattering parameter

$$\alpha = \frac{1}{k\lambda_s} \qquad (2)$$

relates the scattering wave number k to the plasma screening length λ_s (e.g. Debye length for an ideal plasma). A scattering parameter of $\alpha \ll 1$ defines the regime of non-collective scattering whereas $\alpha \gtrsim 1$ results in collective scattering. For a non-collective scattering

geometry, it is relatively simple to decompose the structure factor into three terms [17]:

$$S(k,\omega) = W_{el}(k)\delta(\omega) + W_{b-f}(k,\omega) + W_{f-f}(k,\omega). \quad (3)$$

Here, the first term describes elastic scattering, which is dominated by scattering from tightly bound electrons. The second term accounts for the inelastic scattering from weakly bound electrons and the third term describes inelastic scattering from free electrons. For a carefully chosen scattering geometry, several physical quantities can be deduced from a single scattering spectrum from a particular sample. Particularly, these properties allow for deducing the IPD (bound-free feature), ionization Z (free-free feature in relation to elastic scattering and/or bound-free scattering) and electron temperature T_e (Doppler broadening of free-free feature) from a model fit to a measured spectrum. Furthermore, the ion correlations can be inferred from the ratio of elastic and inelastic scattering, which is highly sensitive to structural transitions, such as melting [18, 19, 20].

3. Synthetic Scattering Spectra

Figs. 1 and 2 show synthetic non-collective scattering spectra for 5.9 keV photon probe energy at a scattering angle of $\theta=160°$ ($k=5.9\,\text{Å}^{-1}$, $\alpha\sim0.2$) for varying ionization (Fig. 1) and electron temperature (Fig. 2) calculated by the XRS code [21] using an estimated instrument function combining the LCLS bandwidth in self-amplified spontaneous emission (SASE) mode and the resolution of the X-ray spectrometer. Since the frequency dependence of the elastic scattering is approximately a delta function on this energy scale, this scattering feature directly reflects the instrument function. Investigating the synthetic spectra on a logarithmic scale, particularly the blue-shifted part of the inelastic scattering on the high-energy side of the elastic scattering is very sensitive to ionization and electron temperature. Moreover, this feature is not obscured by remaining L-shell bound-free scattering since bound-free scattering with positive energy transfer is prevented by the corresponding ionization potential. Thus, an increase in Z at fixed electron temperature results in a linear increase of the scattering intensity on the high-energy side of the elastic scattering. On the other hand, an increase of electron temperature for a fixed Z results in a change in slope of the inelastic feature, since the electron energy distribution is broadened for higher electron temperatures. If the instrument function of the X-ray source and the spectrometer are well characterized over a dynamic range of three orders of magnitude in intensity, ionization and electron temperature of the plasma can therefore be inferred from blue-shifted inelastic scattering with high precision. Fitting the
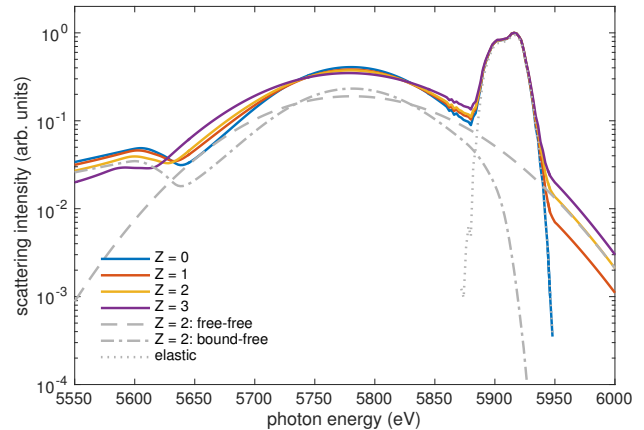

Figure 1. Synthetic scattering spectra for isochorically heated graphite varying Z at $T_e=20\,\text{eV}$. For $Z=2$, the free-free, bound-free and elastic features are shown as well.
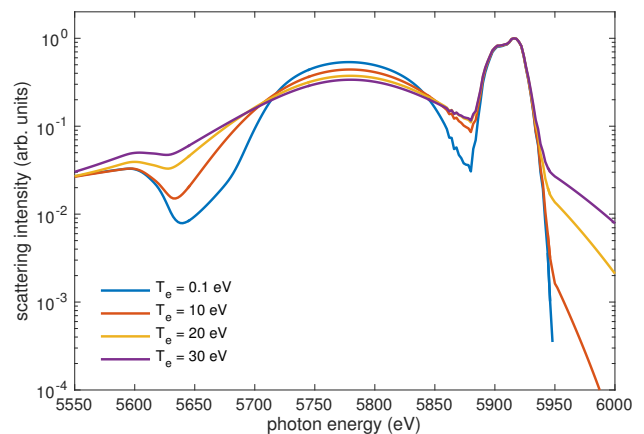

Figure 2. Synthetic scattering spectra for isochorically heated graphite varying T_e at $Z=2$.

rest of the spectrum in addition can serve as a valuable cross-check of applied bound-free models and provide additional information, particularly the K-shell ionization energy and with that the IPD. It should be noted that for low ionization and low temperatures, remaining band structure [22] and chemistry [23] influences the L-shell wave functions and therefore the L-shell bound-free feature. This is not included in the presented single-ion calculations of the electronic structure factor and therefore, all illustrated curves for $Z=0$ and $T_e=0.1\,\text{eV}$ should only be interpreted as rough estimates of the corresponding scattering spectra.

Fig. 3 shows the same synthetic spectra as in Fig. 1, but zoomed in on the carbon K-shell bound-free edge for varying Z at $T_e=20$ eV for two IPD models: Stewart-Pyatt, and modified Ecker-Kroell [3]. The effects of the different models on the K-edge feature are clearly visible. Fig. 4 shows the effect of increasing the initial density, e.g. by using diamond instead of
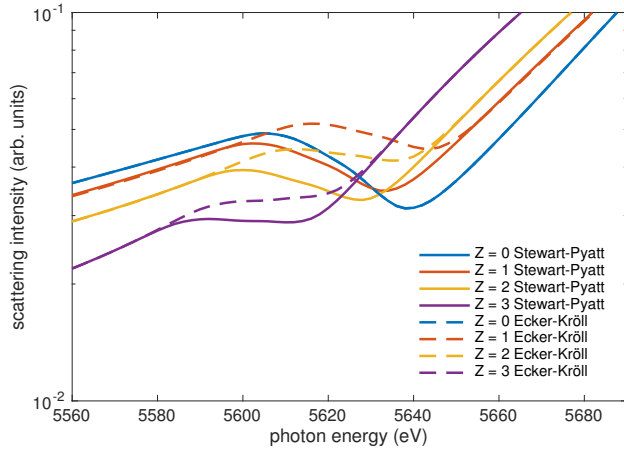
Figure 3. Synthetic spectra for isochorically heated graphite zoomed on the carbon K-shell bound-free edge and varying Z at $T_e=20\,\mathrm{eV}$.
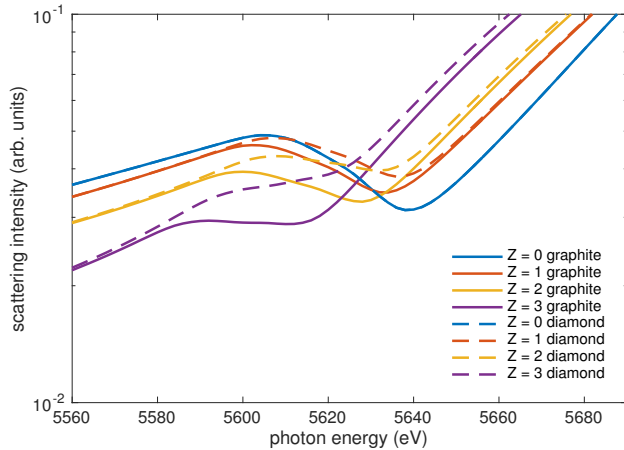

Figure 4. Synthetic spectra zoomed on the carbon K-shell bound-free edge for for varying the plasma density by using graphite and diamond samples.

graphite, which results in a significant increase of the IPD when ionization is present.

4. Experiments

Experimental scattering spectra were obtained at the Matter in Extreme Conditions (MEC) endstation of LCLS [24, 25]. Pyrolytic graphite samples (90 μm thick, initial density ρ_0=2.21 g/cm³) were irradiated by 5.9 keV X-ray pulses of 50 fs in duration and with pulse energies of ∼3 mJ. Using beryllium lenses, the X-ray beam was focussed down to spot sizes below 5 μm in diameter, which results in an estimated peak fluence of up to 3×10^4 J/cm². Around 21.1 % of the incident X-ray flux is absorbed in the sample, which mainly produces K-shell holes and photo-electrons. The range of 5.6 keV photo electrons inside graphite is around 500 nm [26], which is significantly smaller

than the X-ray spot size and ensures that most of the absorbed energy is available to heat the sample inside the X-ray spot. For low-Z elements like carbon, K-shell holes mainly relax by Auger decay which quickly heats the electron subsystem. For the smallest spot size, we estimate that an energy of ∼40 eV is absorbed per atom in the sample volume. Depending on the ionization state, this suggests peak temperatures of the free electrons on the order of 10 eV or more.

The scattered X-rays were collected by a highly annealed pyrolytic graphite (HAPG) crystal spectrometer at a scattering angle of 160°. Fig. 5 shows a spectrum recorded from isochorically heated graphite, which was obtained by accumulating scattering data of 10 separate shots. The elastic and inelastic scattering features can clearly be distinguished. Moreover, the inelastic feature exhibits a clear edge at the low-energy end which originates from the onset of K-shell bound-free scattering and is therefore shifted by the energy required for the ionization of K-shell electrons. A model fit to the scattering spectrum provides a stable fit giving T_e=21.7 eV, Z=1.71, and an IPD of 24 eV. For the free-free scattering we apply random phase approximation (RPA) [21] and the bound-free term is calculated in the impulse approximation (IA) [27] using an effective ionization energy that is given by the atomic binding energy and the plasma-induced IPD. Unfortunately, the required high-precision characterization of the instrument function for accurate measurements of electron temperature and ionization from the blue-shifted part of the free-free scattering is not available for this LCLS proof-of-principle data set. It is only accurate within slightly more than two orders of magnitude and alternate instrument functions with broader wings are also possible (see. Fig. 5). A fit using this modified instrument function provides Z=1.1 and $T_e = 15$ eV, while the IPD remains at 24 eV. Therefore, both Z and T_e can only be stated with a systematic error around 50 %, while the fit error on the IPD is around 5 %. Moreover, the applied bound-free model does not seem to be able to exactly reproduce the shape of the inelastic scattering around its maximum at the Compton energy shift. Nonetheless, the K-shell binding energy and with that the IPD can already be fitted very accurately from the position of the carbon K-shell bound-free edge.

Fig. 6 shows experimental scattering spectra zoomed on the carbon K-shell bound-free edge that were obtained in the described LCLS experiment. For the smallest spot size and thus maximum heating, there is a clear shift of the K-shell bound-free edge towards higher energies that may be induced by increased ionization. Comparing this shift to the trends shown in Fig. 3, where only the modified Ecker-Kroell approach shows a significant shift towards higher energies for
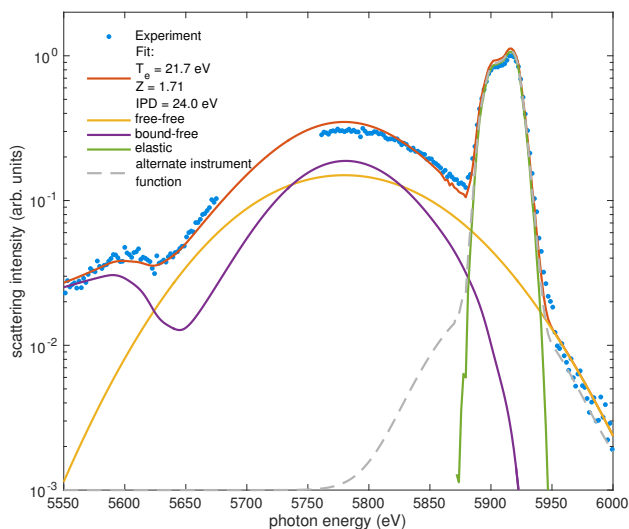
Figure 5. Model fit to experimental data obtained from isochorically heated graphite at LCLS.
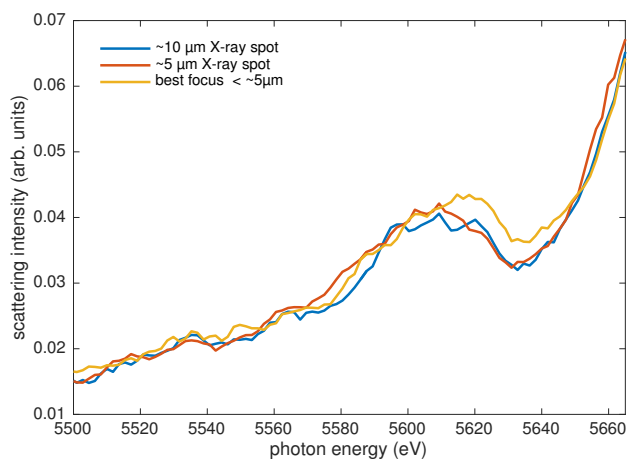

Figure 6. Experimental scattering spectra zoomed onto the carbon K-shell bound-free edge for different X-ray focal spot sizes.

increasing the ionization from 0 to 1 and 2 suggests that the Stewart-Pyatt model indeed underestimates the IPD which is in line with other studies [3, 4, 5]. However, looking at the absolute value of the IPD obtained from the fit (24 eV) is in very good agreement with the Stewart-Pyatt prediction for the best fit plasma parameters (25.3 eV) and does not agree with modified Ecker-Kroell (47.7 eV). For lower ionization, which is well within the error margin of the available data, the situation is different. For $Z = 1$ at the same electron temperature, Stewart-Pyatt predicts 13.3 eV and modified Ecker-Kroell provides 24.6 eV. This underlines the importance of precisely characterizing the ionization state of the plasma as well as the electron temperature for accurate discrimination between models for ionization potential depression in dense plasmas.

5. Conclusions

We have presented an effective method to measure the ionization potential depression in dense carbon plasmas while simultaneously obtaining electron temperature and ionization. Our proof-of-principle experiment performed at LCLS shows that it is in principle possible to record scattering spectra of the required quality. Future experiments will be able to accumulate more spectra for both instrument function characterization and scattering experiments, which will result in the desired accuracy for the blue-shifted free-free scattering and therefore a precise characterization of electron temperature as well as ionization. We have shown that such precision is required to reliably discriminate between ionization potential depression models for dense plasma environments.

Additional information may be obtained by adding collective X-ray scattering at relatively small scattering angles to the experiment. This method can observe electron plasma waves (plasmons) that follow a dispersion relation that is sensitive to density, electron temperature as well as the electron-ion collision frequency [28]. For high dynamic range and sufficiently high temperatures, the electron temperature can also be deduced from comparing the intensity ratio of the upshifted and downshifted plasmon features (detailed balance [29]). However, obtaining precise information on plasmons at dense plasma conditions usually requires very low bandwidth X-ray sources and the relatively broad SASE spectrum may not be sufficient for that. Using self-seeding [30] or monochromators [31] will significantly reduce the X-ray flux available for heating the samples. Moreover, collective scattering can result in ambiguities in the analysis since electron in cold solids or liquids can also be excited collectively (band structure) and corresponding features may obscure the signatures of the free electrons [22].

Finally, it has to be said that for simplicity, the presented analysis and resulting conclusions assume static equilibrium conditions and neglect the dynamic nature of the heating and simultaneous X-ray scattering processes. This simplification can lead to additional ambiguities [32]. However, the influence of heating dynamics can be probed in the experiment by varying the X-ray pulse duration, which can easily be realized at X-ray free electron laser facilities. Another very useful instrument could be the application of the described spectroscopy method to two-color X-ray pump-probe capabilities with varying time delay between the pulses [33].

Acknowledgments

References

[1] V. E. Fortov, *Extreme States of Matter on Earth and in the Cosmos*, Springer (2011).
[2] J. C. Stewart and K. D. Pyatt, Astrophys. J. **144**, 1203 (1966).
[3] O. Ciricosta, et al., Phys. Rev. Lett. **109**, 065002 (2012).
[4] L. B. Fletcher et al., Phys. Rev. Lett. **112**, 145004 (2014).
[5] D. Kraus et al., Phys. Rev. E **94**, 011202(R) (2016).
[6] D. J. Hoarty et al., Phys. Rev. Lett. **110**, 265003 (2013).
[7] S. M. Vinko et al., Nat. Commun. **5**, 3533 (2014).
[8] B. J. B. Crowley High Energy Density Physics **13**, 84-102 (2014).
[9] C. Lin et al., Phys. Rev. E **96**, 013202 (2017).
[10] C. A. Iglesias, High Energy Density Physics **12**, 5-11 (2014).
[11] S. M. Vinko et al., Nature **482**, 59 (2012).
[12] D. Kraus et al., Phys. Rev. Lett. **111**, 255501 (2013).
[13] D. Kraus et al., Nat. Astron. **1**, 606-611 (2017).
[14] O. A. Hurricane et al., Nature **506**, 343 (2014).
[15] J. Sheffield, D. Froula, S. H. Glenzer and J. N. C. Luhmann, *Plasma Scattering of Electromagnetic Radiation*, Academic Press (2011).
[16] S.H. Glenzer and R. Redmer, Rev. Mod. Phys. **81**, 1625 (2009).
[17] J. Chihara, J. Phys.: Condens. Matter **12**, 231-247 (2000).
[18] S. P. Hau-Riege et al., Phys. Rev. Lett. **108**, 217402 (2012).
[19] J. Helfrich et al., High Energy Density Physics **14**, 38-43 (2015).
[20] D. Kraus et al., Phys. Plasmas **22**, 056307 (2015).
[21] G. Gregori et al., Phys. Rev. E **67**, 026412 (2003).
[22] E. J. Gamboa et al., Phys. Plasmas **22**, 056319 (2015).
[23] D. Kraus et al., Phys. Plasmas **25**, 056313 (2018).
[24] B. Nagler, B. Arnold, G. Bouchard, R. F. Boyce, R. M. Boyce, A. Callen, M. Campell, R. Curiel, E. Galtier, J. Garofoli *et al.*, J. Synchrotron Rad. **22**, 520-525 (2015).
[25] S. H. Glenzer, L. B. Fletcher, E. Galtier, B. Nagler, R. Alonso-Mori, B. Barbrel, S. B. Brown, D. A. Chapman, Z. Chen, C. B. Curry *et al.*, J. Phys. B: At. Mol. Opt. Phys. **49**, 092001 (2016).
[26] NIST estar database *https://physics.nist.gov/PhysRefData/Star/Text/ESTAR.html* (2018).
[27] M. Schumacher et al., J. Phys. B: Atom. Molec. Phys., **8**, 1428-1439 (1975).
[28] P. Sperling et al., Phys. Rev. Lett. **115**, 115001 (2015).
[29] S. H. Glenzer et al., Phys. Rev. Lett. **98**, 065002 (2007).
[30] L. B. Fletcher et al., Nat. Photon. **9**, 274 (2015).
[31] D. Shu et al., J. Phys.: Conf. Ser. **425**, 052004 (2013).
[32] D. A. Chapman and D. O. Gericke, Phys. Rev. Lett. **107**, 165004 (2011).
[33] I. Inoue et al., PNAS **113**, 1492-1497 (2016).